ACS APPLIED MATERIALS & INTERFACES

Research Article

www.acsami.org

Permeation of Nickel Nanodots on Carbon Nanotubes: Synthesis of 3D CNT-Based Nanomaterials

Somayeh Mohammadi, Shams Mohajerzadeh,* Azam Gholizadeh, Fatemeh Salehi, and Naser Masoumi

Nano-Electronic Center of Excellence, Thin Film and Nano-Electronic Lab, School of Electrical and Computer Engineering, University of Tehran, Tehran 14395/515, Iran

Supporting Information

ABSTRACT: In this paper, we report the fabrication of three-dimensional (3D) hybrid carbon nanotubes (CNT)-based nanostructures. Secondary carbon nanotubes are grown on the hydrogenated and unzipped horizontal carbon nanotubes without any further catalyst deposition. Hydrogenation of horizontal CNTs leads to out-diffusion of Ni nanoparticles that were trapped within the walls of nanotubes during the original growth process. This out-diffusion effect, as permeation, leads to the formation of nickel dots at the surfaces of carbon nanotubes which acts as the catalyst for the growth of secondary nanotubes. By controlling the secondary growth condition, a variety of 3D structures could be achieved. The permeation effect and the evolution of secondary nanostructures are studied extensively by means of scanning electron microscopy, transmission electron microscopy, atomic force microscopy, X-ray photoelectron spectroscopy, and X-ray diffraction analysis.

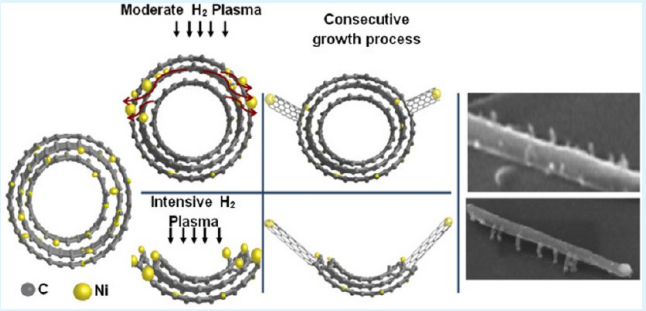

KEYWORDS: *carbon nanotube, Ni nanoparticles, hydrogenation, secondary CNT growth, 3D nanostructures*

INTRODUCTION

Carbon-based nanostructures with sp^2-hybridized atoms such as carbon nanotubes (CNTs), graphene, and graphene ribbons have attracted great attention due to their exclusive properties. Their exclusive properties such as large active surface area, high current density, high thermal and electrical conductivity, and chemical stability have made them promising materials in the fields of electronics, gas sensing and biodetection, energy storage devices, and catalytic applications.[1−6] Recently, there have been several efforts in the field of carbon-based hybrid nanomaterials. Decorated carbon nanotubes with Ni particles[7−10] and graphene supported Ni/carbon composites[11−13] have been extensively studied due to their improved electrochemical sensing, catalytic properties,[8,10] and hydrogen storage.[11,14,15] Most of the preparation methods for these materials are based on the deposition of metal particles on the functionalized surface of carbon nanotubes and graphene in a Ni containing solution.[7,11,16]

Apart from metal/carbon hybrid materials, recent studies are being pursued to synthesize three-dimensional carbon-based nanostructures.[16−22] The outstanding properties of different carbon nanomaterials has made such hybrid nanostructures attractive for applications in a variety of fields such as energy storage devices, super capacitors, electrochemistry, and optoelectronics.[17,19−21,23] Most of the reported fabrication methods involve the growth of carbon nanotubes on the hydrogenated catalyst layer deposited on the surface of a graphene sheet.[17−19] Other methods are solution-based approaches[20,22] or innovative processes such as the one introduced by Dong and co-workers, who synthesized graphene−carbon nanotube hybrid materials by a one-step chemical vapor deposition (CVD) on a copper foil decorated with silicon nanoparticles.[16] A few works have also been reported on the fabrication of CNT−CNT structures by means of the Ni catalyst deposited on the walls of primary CNTs[24] or hydrogenation of the Ni on the tip of primary vertical CNTs and applying a secondary growth process to obtain tree-like structures.[25]

In this article, the fabrication of three-dimensional CNT−CNT and graphene nanoribbon (GNR)−CNT nanostructures is reported. By applying a controlled hydrogenation process to horizontal carbon nanotubes followed by an appropriate growth process, the growth of secondary nanotubes attached to the primary ones is feasible. A variety of CNT−CNT and GNR−CNT structures could be achieved by modifying the growth process. By controlling the growth condition, we can prevent the etching of underlying carbon-based structures during the growth of secondary nanotubes.

No catalyst deposition is needed for the growth of secondary nanotubes. We have observed an anomalous leaching of the nickel atoms toward the outer surfaces of the primary horizontal nanotubes during the hydrogenation process. This

Received: June 17, 2014
Accepted: August 17, 2014
Published: August 17, 2014

   dx.doi.org/10.1021/am5038565 | ACS Appl. Mater. Interfaces 2014, 6, 15352−15362

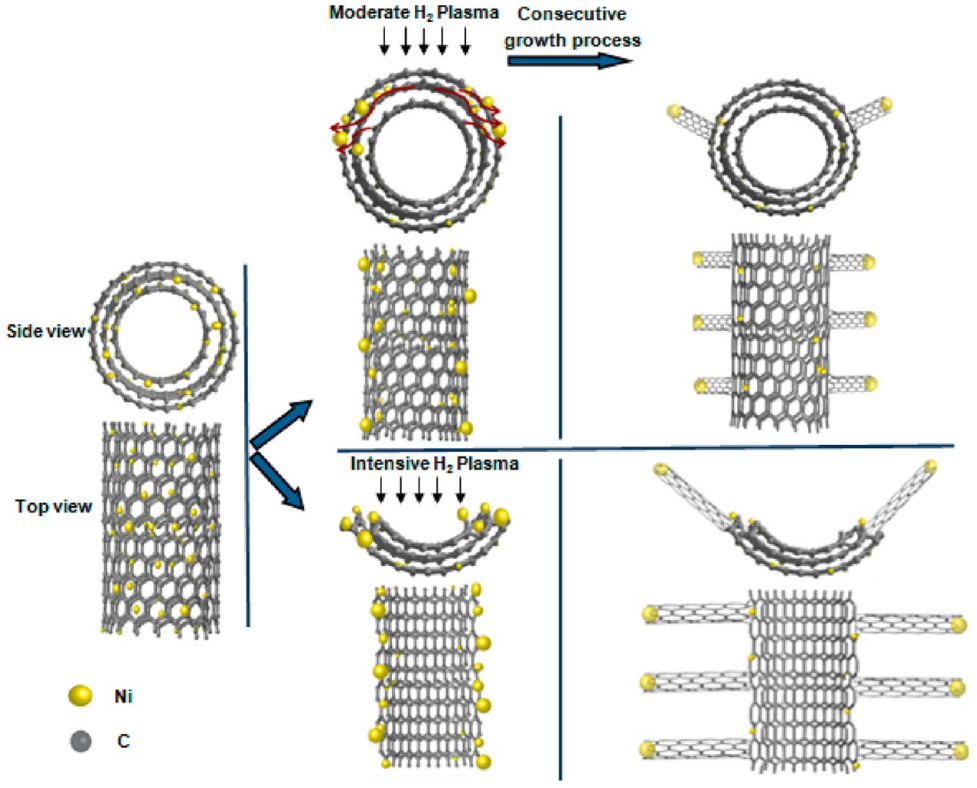

Figure 1. . Schematic illustrating the steps of plasma-assisted nickel nanodots out-diffusion and lateral CNT growth. Red arrows show the trajectory of Ni nanodots during hydrogenation. The formation of nickel nanoparticles is believed to be due to the migration of nickel from inside the layers toward the outer surfaces. Such agglomeration is observed in microscopy images. The intensive plasma exposure leads to both migration of Ni and unzipping of nanotubes as well as the formation of graphene ribbons.

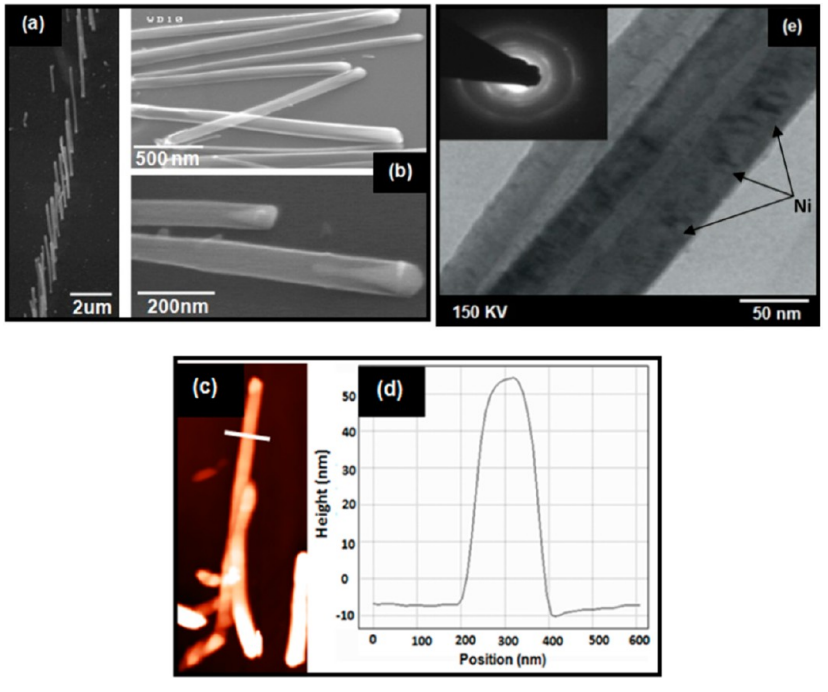

Figure 2. (a) SEM images of as-grown vertically aligned and (b) transformed horizontally aligned CNTs. (c) AFM image of horizontal CNTs, (d) height profile of the line assigned in the AFM image in panel c, (e) TEM images of as-grown CNTs, and (e, inset) diffraction pattern of the CNTs.

out-diffusion of nickel would lead to the formation of nickel nanodots at the outer surfaces of CNTs that could play the role of catalyst for the growth of secondary CNTs. Permeation of Ni nanodots also enhances the previously reported unzipping of carbon nanotubes.[26] We have investigated the effect of hydrogenation on the out-diffusion of Ni nanodots and the role of these Ni particles on the unzipping of carbon nanotubes. We have also investigated the effect of hydrogenation on the

dx.doi.org/10.1021/am5038565 | ACS Appl. Mater. Interfaces 2014, 6, 15352−15362

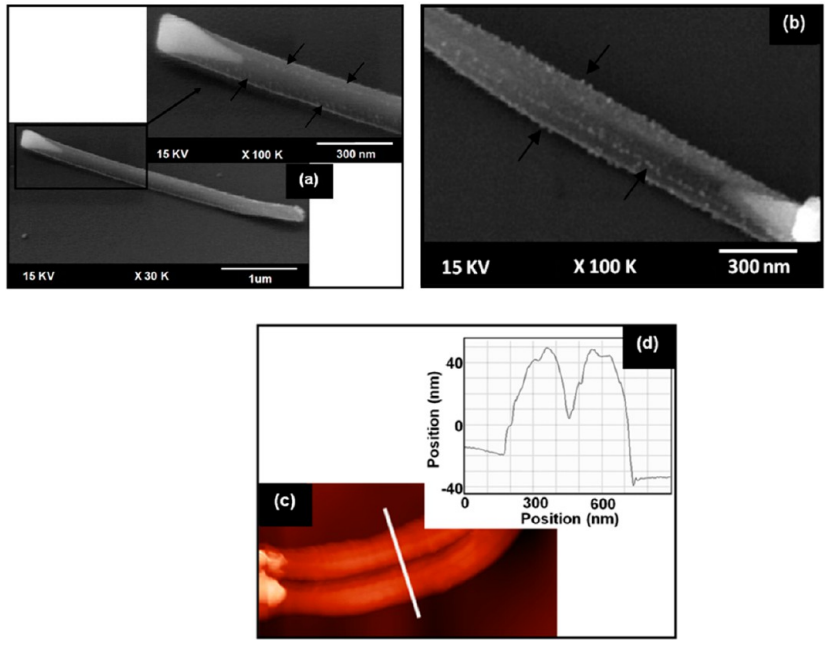

Figure 3. SEM images of CNTs exposed to hydrogenation process for (a) 10 and (b) 30 s at 600 °C with a hydrogen flow of 20 sccm and plasma power of 0.5 W cm^{-2}. (c) AFM image of two adjacent CNTs exposed to the same hydrogenation process as the one in panel b. (d) Height profile of the white line in panel c. (a and b) Black arrows show the Ni nanodots on the surface of carbon nanotubes.

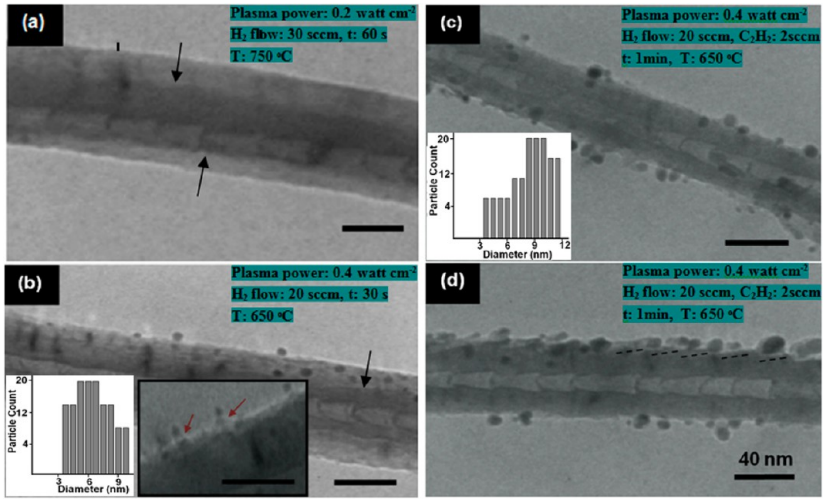

Figure 4. TEM images of hydrogenated CNTs at different conditions. (a and b) Black arrows mark the boundary of swelled outer shells and intact inner shells, and (b, right inset) brown arrows mark very short CNTs that grow in H_2 plasma. Histograms depict the distribution of Ni nanoparticle sizes formed in (b, left inset) H_2 and (c, inset) H_2 + C_2H_2 ambient. (d) Dashed lines show the trajectory of Ni nanodots during out-diffusion.

electrical behavior of horizontal CNTs. Scanning electron microscopy (SEM), transmission electron microscopy (TEM), atomic force microscopy (AFM), X-ray photoelectron spectroscopy (XPS), and X-ray diffraction (XRD) analyses have been used to study such nanostructures.

EXPERIMENTAL METHODS

Vertically aligned multiwall carbon nanotubes with diameters of 50−100 nm are synthesized. Prior to the growth of CNTs, a layer of nickel with a thickness of 10−12 nm was deposited on the substrate to act as the catalyst layer. The nickel-coated substrate is placed in the DC-PECVD reactor under hydrogen flow of 20 sccm. Ni catalyst is annealed in hydrogen ambient for 30 min at 680 °C. After a 5 min hydrogenation step with the plasma power of 2 W/cm^2, we start the growth process by introducing C_2H_2 gas with the flow rate of 4.5 sccm. Plasma power is 2.5 W/cm^2 during the growth process.

The synthesized vertically aligned CNTs are transferred to another clean silicon substrate in horizontal manner using the procedure explained in our previous works.[27,28] Horizontal CNTs are then exposed to moderate hydrogen plasma with the power of around 0.4 W/cm^2 at a temperature of 500−650 °C. Under these conditions, Ni species appear on the surface of carbon nanotubes. Increasing the plasma power to 0.7 W/cm^2 would lead to unzipping of carbon nanotubes. These nanotubes could experience a secondary growth process either in vertical or horizontal DC plasma at a temperature of 600−850 °C. In the case of horizontal plasma, the samples are placed on a piece of quartz plate, and plasma is established through two stainless electrodes on the sides of the plate. Under proper conditions, secondary nanotubes would grow and connect to the primary horizontal nanotubes. A schematic illustrating the steps of Ni nanodots formation and secondary CNT growth is presented in Figure 1.

For electrical measurement, a thin layer of SiO_2 with a thickness of 150 nm was thermally grown on a Si wafer at 1300 °C in oxygen

ambient in a quartz tube. A thin layer of Mo with a thickness of 50 nm was then deposited on the SiO_2 surface by means of RF-sputtering. According to the theoretical calculation of Dang et al. carbon nanotubes are strongly side-bonded to the Mo surface, resulting in Ohmic contact and significant charge transfer.[29] The Mo layer was patterned using a photolithography process to obtain two electrodes with an oxide layer as the gap between them. CNTs were individually placed on the electrodes perpendicular to the gap.

RESULTS AND DISCUSSIONS

Permeation of Ni Nanodots. The characteristics of as grown CNTs are examined by means of SEM, AFM, and TEM as collected in Figure 2. According to SEM and TEM images, the surface of CNTs is smooth without any observable Ni particles on them. The height profile of the AFM image in Figure 2d confirms the smoothness of the CNT surface. Dark lines and dots in the TEM image are attributed to Ni clusters entrapped within the CNT structure during the growth process. We surprisingly observed that by applying a controlled modest hydrogenation process, entrapped Ni nanoparticles diffuse out of the structure and form Ni nanodots on the outer surfaces.

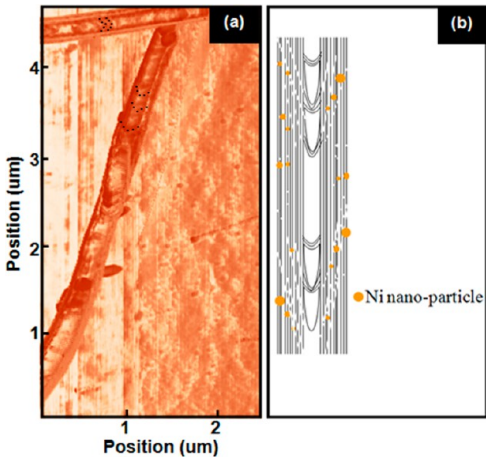

Figure 5. (a) AFM phase image of two slightly hydrogenated carbon nanotubes. A conductive (TiN) noncontact tip is used to observe the internal structure of carbon nanotubes. (b) Schematic illustrating defect lines of a CNT correspondent to the CNTs shown in panel a.

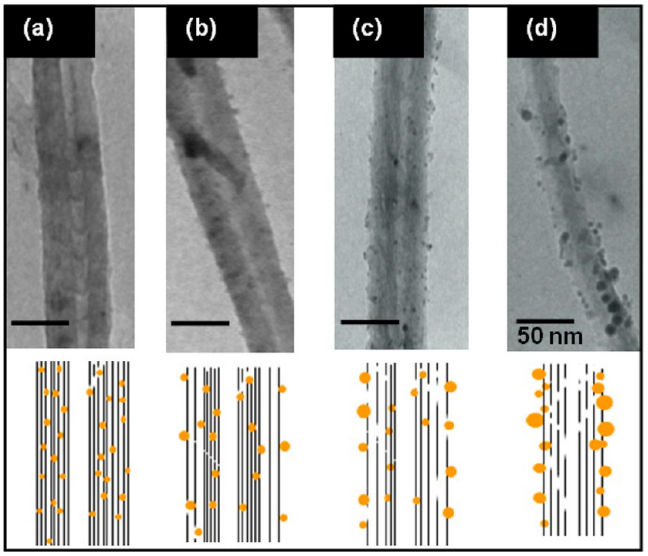

Figure 6. (a–d, top) TEM images and (bottom) schematics representing the evolution steps of the formation and permeation of Ni nanoclusters during hydrogenation. Hydrogenation durations were (b) 10, (c) 30, and (d) 50 s. (a) Nickel atoms are randomly distributed; (b and c) nickel atoms start to move outward and form nanosize clusters of nickel; and (d) the evolution of nickel nanoparticles is completed on the outer surfaces of the nanotubes.

In Figure 3, SEM and AFM images of CNTs exposed to hydrogen plasma with the hydrogen flow of 20 sccm and plasma power of 0.4W/cm^2 at a temperature of 600 °C are presented. As seen in these SEM images, the surfaces of the nanotubes are decorated by Ni nanodots. The hydrogenation time experienced by CNTs in Figure 3, panels a and b, were 10 and 30 s, respectively. Longer hydrogenation times leads to more Ni nanodots formation on the surface of carbon nanotubes. However, continuing the hydrogenation process for more than 30 s leads to unzipping or etching of carbon nanotubes. Two adjacent nanotubes exposed to the same hydrogenation condition as the one in Figure 3b, are presented in the AFM image in Figure 3c. The roughness of the height profile in Figure 3d is the result of the formation of Ni nanodots and partial rupture of the outer shells due to hydrogen plasma. The density and the size of Ni nanodots on the surface is dependent on the hydrogenation parameters, especially plasma power and exposure time.

The effects of hydrogenation parameters on the formation of Ni nanodots are depicted in the TEM images in Figure 4. The CNT shown in Figure 4a is hydrogenated with low plasma power but at high hydrogen pressure and high temperature. Due to low plasma power, no Ni nanoparticle formed on the surface. Elevated temperature and high hydrogen pressure merely lead to more adsorption and storage of hydrogen atoms onto carbon nanotube structure and, consequently, the exfoliation of CNT walls. Enhanced plasma power results in out-diffusion of Ni particles in addition to enlargement of the CNT, which could easily happen, even at a lower temperature and pressure (Figure 4b). We believe that under appropriate hydrogen plasma, entrapped Ni particles become active and move toward the outer surfaces and merge to form larger islands. They can break up the C−C bonds through their path, which in turn facilitates their movement. Exfoliation of the shells is another expediting parameter for the movement of the Ni grains. It was observed that a very short growth of CNTs could happen on the out-diffused Ni dots during hydrogenation. These CNTs are marked by brown arrows in the SEM image in the inset of Figure 4b. On the basis of the surface etching and bond breaking of the primary horizontal carbon nanotubes in the hydrogen plasma, we speculate that hydrocarbonic gases (C_nH_m) are locally produced. Local pyrolysis of these gases by means of Ni nanodots as catalyst particles leads to the growth of secondary short CNTs. Another interesting observation is the constructive contribution of acetylene gas in the formation of Ni nanodots. TEM images in Figure 4c,d correspond to the Ni nanodots formation in the presence of C_2H_2. By comparing these images with that in Figure 4b, it is observed that Ni nanoparticles leach out more noticeably and with larger sizes in the presence of C_2H_2. The size distribution histograms of Ni dots in the insets of Figure 4b,c confirm the effect of C_2H_2 on the enlargement and more out-coming of Ni nanoparticles. Currently, the constructive role of hydrocarbonic feedstock in the formation of Ni nanoclusters is not fully understood. The dashed lines in Figure 4d show the routes of nickel clusters during out-diffusion. These lines originate

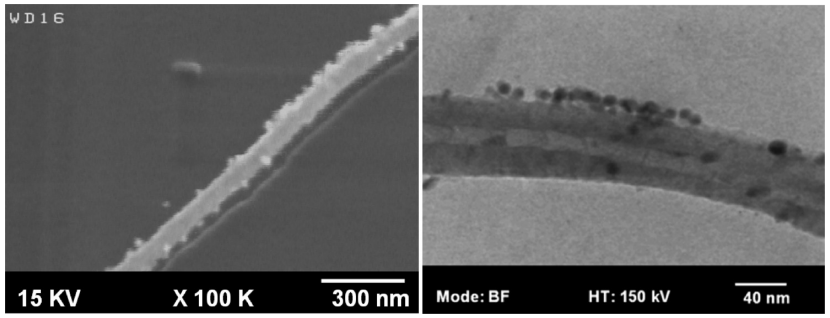

Figure 7. (a) SEM and (b) TEM images of hydrogenated CNTs in the presence of 2 sccm C_2H_2 gas. The hydrogenation duration was 50 s, the same as that for the CNT in Figure 6d. The formation of larger nickel nanoclusters is quite evident in these images.

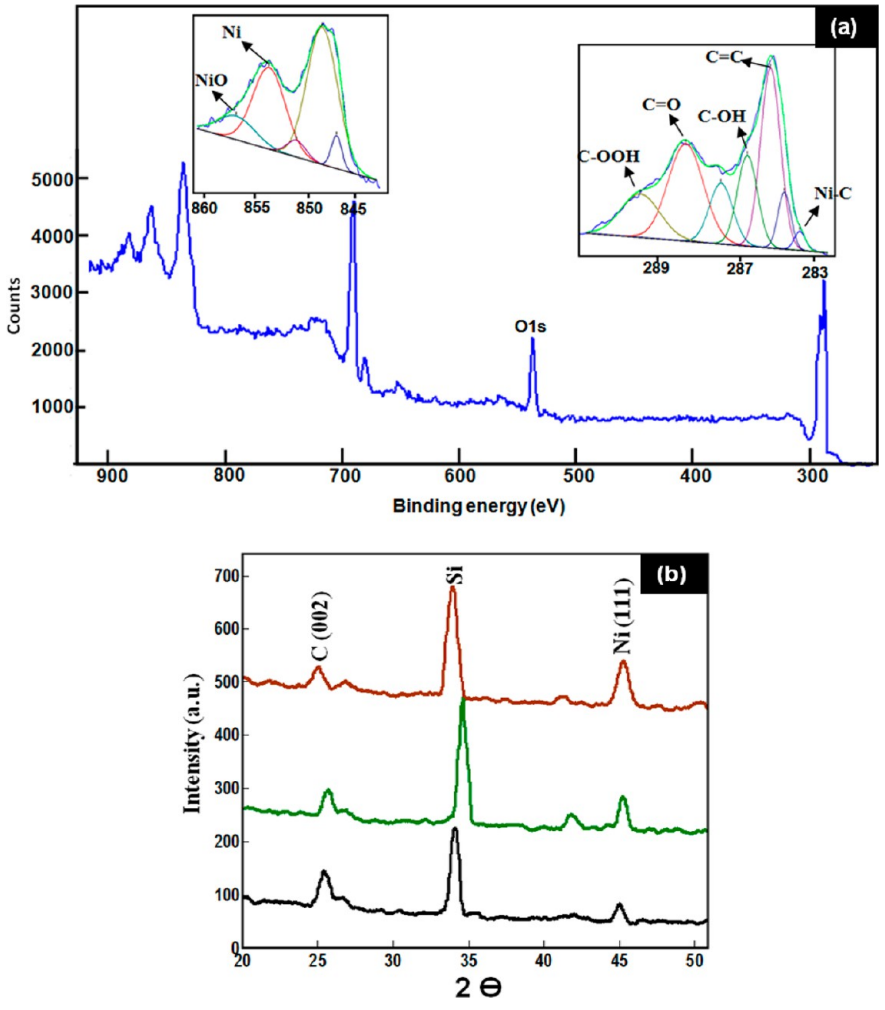

Figure 8. (a) XPS data for the multiwall carbon nanotubes to show the nickel−nickel and nickel−carbon bonds. By deconvolution of the spectra, a small shoulder peak due to Ni−C bonds is extracted at 283.5 eV. (b) The XRD analysis of the hydrogenated nanotubes suggests the presence of agglomerated nickel particles; (black) horizontal CNTs not exposed to hydrogenation; samples exposed to hydrogenation for (green) 2 and (red) 4 min and with the plasma power of 0.3 W/cm^2 at 500 °C. These data corroborate with the SEM images of the samples in which agglomerated features are well observed on the outer surfaces of the nanotubes.

from the bamboo-shaped structure of the inner tubes, extend to the outer surfaces, and indicate the preferable paths for the motion of nickel atoms. These paths are more discernible in the AFM phase image in Figure 5a. For this experiment, we have used a conductive noncontact tip, which enabled us to observe the internal structure of carbon nanotubes in the phase image. The movement of Ni particles through defect lines is schematically illustrated in Figure 5b. Although it is not possible to arrive at a comprehensive theoretical model for the out-diffusion of nickel clusters and atoms, we speculate that the inclusion of hydrogen ions inside the nanotube (during hydrogenation) would lead to an induced electric field, which can enhance the motion of nickel atoms and clusters toward the outer surfaces.

The formation steps of Ni nanodots under mild hydrogen plasma (with the plasma power of 0.4 W/cm^2) are presented in

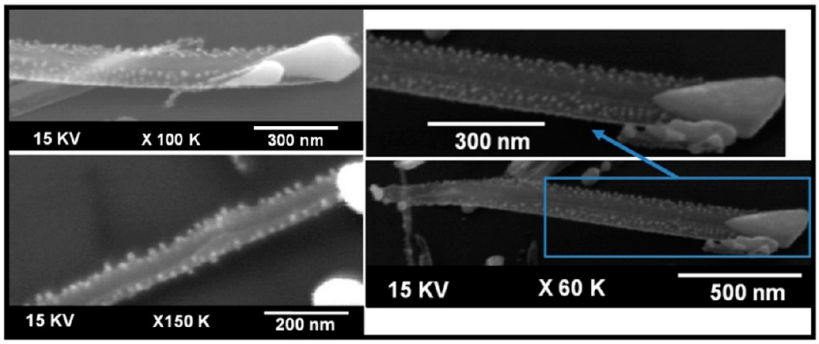

Figure 9. SEM images of unzipped CNTs due to strong hydrogenation process in a short time. White dots on the edges of graphene nanosheets are Ni nanoparticles.

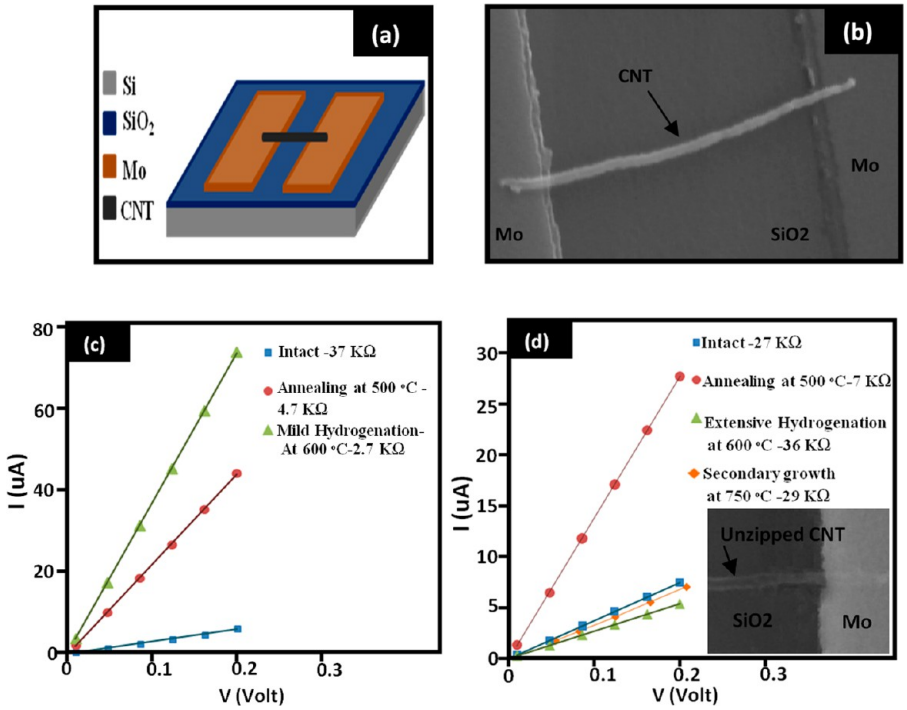

Figure 10. (a) Schematic and (b) SEM image of the device fabricated to study the electrical characteristics of processed CNTs. (c and d) *I*−*V* diagrams of two samples after annealing and hydrogenation; the variation of the diagrams shows (c) slight hydrogenation and (d) extensive hydrogenation. (d, inset) SEM image of the unzipped CNT with the *I*−*V* behavior presented in panel d. The secondary growth at 750 °C has led to a slight increase in the sample current (drop in its electrical resistance), which could be due to partial removal or passivation of defect sites during the second growth.

Figure 6. As depicted in the schematic of Figure 6a, before being exposed to the hydrogenation process, Ni atoms and particles are distributed within the CNT walls. At the early stages of hydrogenation, a few Ni nanoparticles with ultrasmall sizes emerge on the surface of carbon nanotubes (Figure 6b). These Ni particles were primarily trapped in the outer layers of CNT walls. We speculate that agglomeration and permeation of these nanodots are assisted by the swelling and partial C−C bond breaking of the outer shells. As the hydrogenation continues, more Ni nanodots appear on the surface (Figure 6c). We believe that hydrogen ions gradually diffuse into the inner walls of the CNTs and lead to the exfoliation and C−C bond breaking of the inner shells. Hence, the movement, agglomeration, and out-diffusion of inner layer entrapped Ni particles are facilitated. At this stage, partial etching of outer walls is inevitable due to the extended plasma exposure time. When the hydrogenation process time increases, CNT walls are etched more while the entrapped Ni atoms and nanoparticles remain. These particles would easily agglomerate and appear on the surface with large sizes (Figure 6d). No carbon feed-stock was present in the process applied to the CNTs of Figure 6. In Figure 7, one can see the SEM and TEM images of some nanotubes, which have been hydrogenated in the presence of 2 sccm C_2H_2 (acetylene) gas with the same hydrogenation duration of the samples depicted in Figure 6d. As is visible in these images, the presence of a small amount of a carboneous gas leads to the formation of large Ni clusters on the surface without etching the CNTs.

The presence and the agglomeration of Ni particles within the CNT structure are approved by means of XPS and XRD analyses. The XPS analysis of as-grown multiwalled carbon nanotubes (MWCNTs, Figure 8a) demonstrates the contribution of Ni in the structures of nanotubes. Two peaks at 852.9 and 283.5 eV correspond to the Ni−Ni[7,15] and Ni−C[29] bonds,

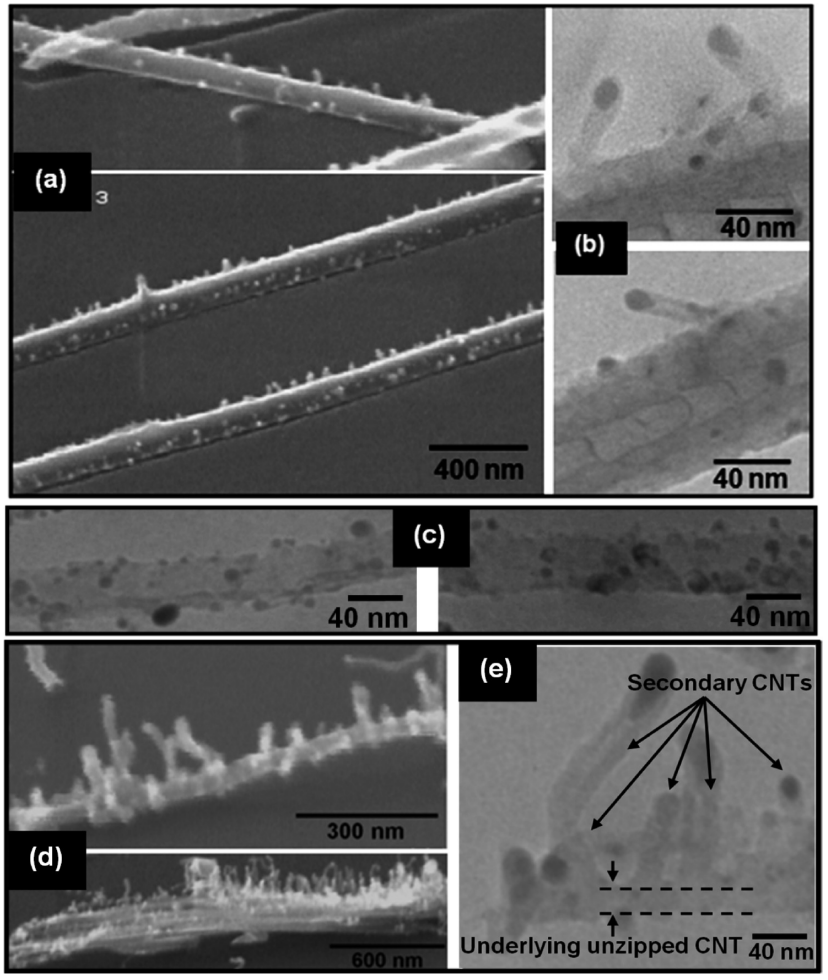

Figure 11. (a) SEM and (b) TEM images of 3D CNT−CNT, and (c) TEM images of unzipped CNTs. Black dots in these images are Ni nanoclusters. (d) SEM and (e) TEM images of 3D GNR−CNT structures obtained in vertical plasma at 650 °C. The flow rate of C_2H_2 and H_2 were 4 and 20 sccm, respectively. (e) The layer between two dashed lines is the primary unzipped CNT. The black arrows mark secondary nanotubes.

respectively, which indicate the existence of Ni particles bonded to carbon atoms. The peaks at 286.7, 288.2, and 289.5 eV are attributed to C−OH, C═O and C−OOH groups, respectively.[30] The existence of these groups is related to the absorbance of oxygen gas in the air ambient while the samples are taken out of the chamber and carried over to the XPS analysis apparatus. The XRD patterns of intact horizontal CNTs and hydrogenated ones for 2 and 4 min are presented in Figure 8b. By precisely comparing these three patterns, we can see that the intensity of the peak at 45.2° is stronger in hydrogenated samples. In addition, we observe that longer hydrogenation time leads to a more intense peak. Because the peak at 45.2° corresponds to Ni with (111) orientation,[7,11] the observed increase in its intensity corroborates the agglomeration and crystallization of Ni nanoparticles during hydrogenation post processing.

It is worth mentioning that nickel clusters can dissolve carbon atoms while moving, which in turn leads to etching and unzipping of CNTs in strong hydrogen plasma. By applying an extensive hydrogenation process (with the plasma power of about 0.7 W/cm^2) during a short time (about 15 s), the unzipping of carbon nanotubes is inevitable (Figure 9). Ni capability to cut out graphene and CNTs has been previously studied by Ci et al.[31] and Elias et al.,[32] respectively. In both cases, Ni particles have been deposited on the graphene and carbon nanotube surfaces and the activation of Ni particles and cutting process occurred at high temperatures (750−1100 °C) in an Ar−H_2 atmosphere. However, by applying hydrogen plasma, one could activate Ni nanodots at a lower temperature (500−650 °C), which could lead to complete longitudinal unzipping of nanotubes. Apart from the role of Ni particles in direct bond breaking, the presence of Ni increases the hydrogen storage capability within the CNT structure, dramatically.[33−35] This capability is improved as the size of Ni particles is decreased.[36] Hydrogen storage leads to more swelling of the CNT, which has two important consequences: exfoliation of the CNT shells and induced structural strain resulting in the weakening of the C−C bonds and facilitating the proper unzipping process.

Current−Voltage Characteristics. The current−voltage (I−V) characteristics of intact, slightly hydrogenated and unzipped CNTs are studied in this part. As presented in the schematic and SEM images in Figure 10a,b, an individual CNT is horizontally placed on Mo pads. It was observed that annealing at temperatures higher than 200 °C in the hydrogen atmosphere reduces the resistivity of the structures quite significantly. This tremendous reduction could be attributed to the improvement of CNT and Mo pads side-contact quality. The annealed structures are divided into two groups exposing mild and extensive hydrogen plasma. The electrical con-

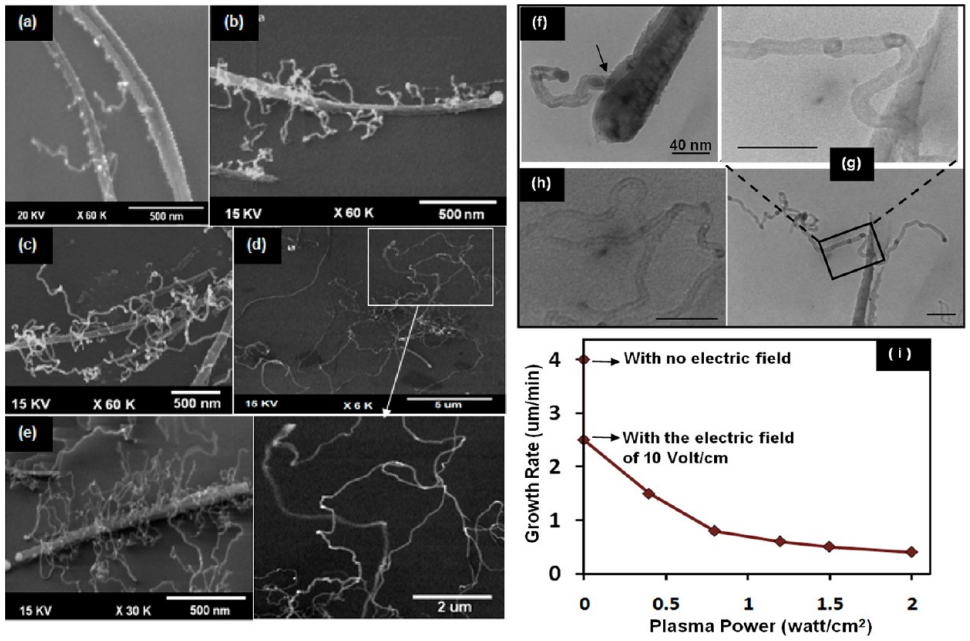

Figure 12. SEM images of secondary nanotubes grown at 850 °C with the plasma power of (a) 1.6, (b) 0.8, (c) 0, (d) 0, and (e) 0 W/cm^2. (c) A horizontal electric field with a magnitude of 10 V/cm is applied. (e) During the secondary growth process, 1 sccm of nitrogen is introduced to the system. (f–h) TEM images of secondary narrow diameter tubes, (i) diagram of the growth rate versus plasma power. The flow rate of C_2H_2 and H_2 are 4 and 25 sccm, respectively, in all cases. As observed the plasma power inversely affects the growth rate.

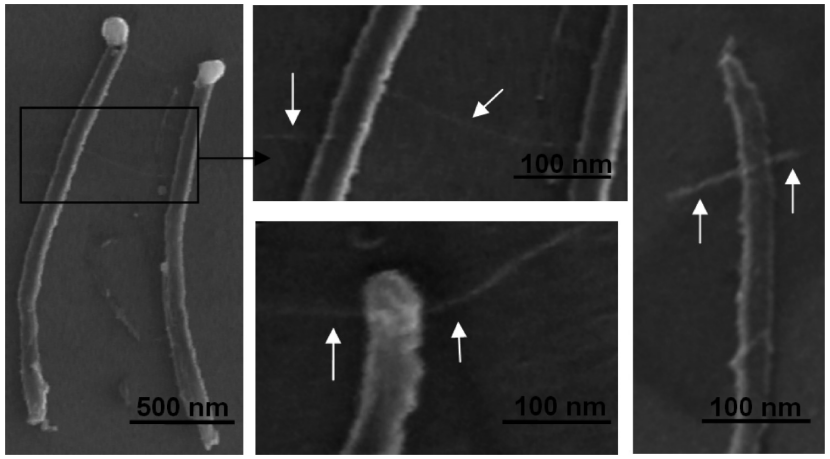

Figure 13. A collection of SEM images of ultranarrow, straight secondary CNTs. The estimated diameter of secondary CNTs is 2–6 nm. The white arrow in the middle top image shows a traversing thin nanotube between neighboring CNTs.

ductivity is increased in the first group, while it is dramatically decreased in the second group. The $I-V$ characteristics of two slightly and extensively hydrogenated samples are presented in Figure 10, panels c and d, respectively. We believe that exfoliation of CNT walls is mainly responsible for resistivity decrement in the slight hydrogenation process. Exfoliated CNT shells can act more like a one-dimensional conductor with less scattering effect. Migration of Ni atoms from within the walls to the surface could be another reason for scattering reduction. On the contrary, conductivity reduction in unzipped CNTs could be primarily attributed to scattering from defective open edges. For the unzipped sample, which has been exposed to a secondary growth, the electrical resistance shows a modest decrease, as seen in the inset of Figure 10d. Although the reason for the resistance reduction is not clearly understood, it can be related to defect removal in the presence of a carbon feed-stock. The passivation of the defect sites by amorphous carbon during the secondary growth process could partially enhance the electrical performance of the unzipped structures.

Three-Dimensional Growth. Ni nanodots that appear on the surface of carbon nanotubes and on the edges of produced graphene nanosheets have the potential to act as the catalyst for the further CNT growth. Pursuing the hydrogenation step by a proper growth process, anomalous three-dimensional CNT–CNT and GNR–CNT nanostructures are obtained. By adjusting the secondary growth conditions, the characteristic parameters of secondary nanotubes including their diameter, length, growth rate, and direction are controlled. Depending on the direction of plasma, the growth of secondary nanotubes perpendicularly or laterally connected to the primary tubes is feasible. Process temperature, the ratio of C_2H_2/H_2, and the plasma power are other parameters that affect the structure of secondary tubes. A collection of SEM and TEM images of secondary nanotubes grown in vertical plasma is presented in

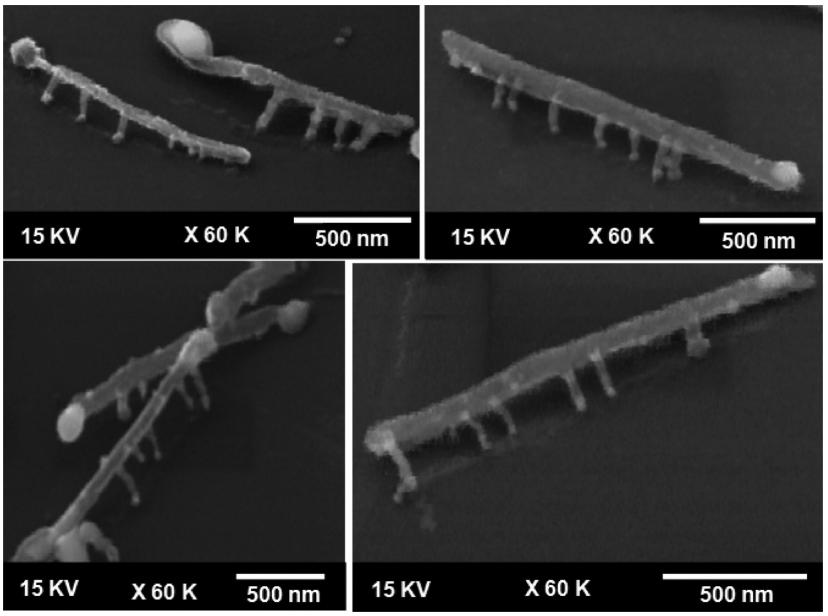

Figure 14. SEM images of 3D insect-like structures. The primary tube has been laid down and the secondary features are grown to incorporate short "legs" onto the original tube. With a flow rate of 6 sccm of C_2H_2 and 20 sccm of H_2 and plasma power of 2 W/cm^2, secondary tubes grow downward from the bottom of the CNTs, and as a result, the primary tube is lifted up.

Figure 11. Due to the vertical direction of plasma, secondary nanotubes grow in a vertical manner. In Figure 11a,b, the secondary grass-like CNTs are perpendicular to the primary one. TEM images of unzipped CNTs are depicted in Figure 11c. Black dots in these images are Ni nanoclusters. In Figure 11d,e, secondary vertical CNTs grown on the underlying unzipped nanotubes are visible. The plasma power in the secondary growth process is lower than the primary one so that the underlying CNT or graphene sheets are not etched away. By increasing the growth temperature to 850 °C and applying a horizontal plasma, lateral and narrow diameter tubes could be achieved. At this temperature, the distribution and the growth rate of secondary nanotubes can be modified by altering the plasma power. A collection of SEM and TEM images of secondary nanotubes grown at a temperature of 850 °C are depicted in Figure 12. According to the presented SEM images, plasma has a deterring effect on the growth rate of lateral CNTs. With no plasma and no electric field, the growth rate of CNTs would be more than 4 μm/min. Despite the increment in the growth rate, the laterality of nanotubes is degraded in the absence of a horizontal electric field and plasma. The diameter of secondary tubes are usually around 10−15 nm. Smaller diameters could be achieved by introducing a tiny amount of nitrogen during the growth process. In this case, the density of secondary tubes markedly increases (Figure 12e). We suggest that incorporation of nitrogen would affect the agglomeration of Ni dots on the surface of the underlying primary CNT, which in turn results in high density and low diameter secondary tubes. Activated nitrogen would enhance the rate of graphitic layer nucleation on the surface of catalyst grain[35,36] and consequently passivates the Ni spots and prevents them from further agglomeration.

Referring to TEM images in Figure 12, one can observe the diameter size and the inner structure of secondary tubes more clearly. The black arrow in Figure 12f, points at the interface of secondary tube and the graphitic layer of underlying CNT. In Figure 12g, a high aspect ratio tube grown at the edge of an unzipped CNT is presented. The wall thickness of the long CNT depicted in Figure 12h is about 2 nm which implies that its number of shells is less than six. The diagram in Figure 12i depicts the effect of plasma and electric field on the growth rate of lateral tubes. According to this diagram, at high plasma powers, the sensitivity of the growth rate to plasma power is lowered. This could imply that at an elevated plasma power, the deteriorating effect of the electric field at the growth rate is compensated by more decomposition of carbon feedstock. All of the above structures comprising a conductive underlying CNT connecting to narrow diameter, long branch-like tubes are good candidates to be used in energy storage devices such as batteries and super capacitors. Apart from spaghetti-like structures, straight, ultranarrow secondary tubes with a diameter less than 6 nm are also observed. These CNTs are marked by white arrows in the SEM images in Figure 13. We speculate that high temperature and low pressure assist the formation of such structures. More investigation on the formation of these branched structures is in progress.

As we increase the C_2H_2/H_2 ratio, completely different 3D, insect-like structures form (Figure 14). We set the flow rate of C_2H_2 and H_2 to 6 and 20 sccm, respectively, and apply a horizontal plasma with an increased power of 1.5−2 W/cm^2, causing Ni particles to come out from the bottom side of primary CNTs, and the secondary tubes grow toward the substrate to incorporate short "legs" onto the original tube. Referring to Figure14, we see that primary CNTs are up-lifted by the connecting leg-like secondary tubes. These structures have the capability to walk if they could get free from the substrate. No insect-like structure is feasible if the flow rate of acetylene or the power of plasma is reduced. This observation suggests that enhanced decomposition of carbon feedstock plays an important role in the emerging of leg-like tubes.

CONCLUSIONS

In summary, agglomeration of nickel nanodots on the outer surfaces of carbon nanotubes has been observed and studied

after nanotubes have been exposed to a modest hydrogenation process. The intensive exposure of nanotubes to hydrogen plasma leads to the unzipping of carbon nanotubes, but a modest low-energy process results in an out-diffusion of nickel particles to outer surfaces of the CNTs without any damage to the primary structure. The source of nickel is believed to be the trapped nickel atoms within the walls of carbon nanotubes during the primary growth process. This out-diffusion is permeation of nickel atoms from their original place toward the outer surface, a process that is enhanced by hydrogenation. Study of the electrical conductivity of the structures shows an enhanced performance after mild hydrogenation. Nanosized Ni dots can be used as catalyst for further growth of lateral carbon nanotubes. Either vertical or horizontal secondary tubes could be achieved by controlling the secondary growth condition. Secondary CNTs are extremely thin in diameter and could grow with the rate of as much as 4 μm/min. Apart from lateral thin-diameter secondary tubes, 3D insect-like structures could be obtained by modifying the secondary growth parameters. The formation of secondary growth could be suitable for ion-batteries and supercapacitors where the carrier transport of ions in the electrolyte plays a crucial role in overall performance of the device. Moreover, the fabrication of ion-based sensors is feasible by the partially interdigital structure of the 3D secondary nanotubes. The work on lithium ion batteries and supercapacitors based on unzipped carbon nanotubes is underway.

■ ASSOCIATED CONTENT

Supporting Information

The Raman spectra of intact, slightly hydrogenated, and unzipped CNTs. This material is available free of charge via the Internet at http://pubs.acs.org.

■ AUTHOR INFORMATION

Corresponding Author

*Tel/Fax: +9821-88011235. E-mail: mohajer@ut.ac.ir.

Notes

The authors declare no competing financial interest.

■ ACKNOWLEDGMENTS

The authors wish to acknowledge the technical support of R. Talebi, S. A. Hoseini, and S. Soleimani for electron microscopy. This work has been partially supported by the Research Council of the University of Tehran.

■ REFERENCES

(1) Geim, A. K.; Novoselov, K. S. The Rise of Graphene. *Nat. Mater.* **2007**, *6*, 183−191.

(2) Geim, A. K. Graphene: Status and Prospects. *Science* **2009**, *324*, 1530−1534.

(3) Bolotin, K. I.; Sikes, K. J.; Jiang, Z.; Klima, M.; Fudenberg, G.; Hone, G.; Kim, P.; Stormer, H. L. Ultrahigh Electron Mobility in Suspended Graphene. *Solid State Commun.* **2008**, *146*, 351−355.

(4) Peigney, A.; Lauren, T. C.; Flahaut, E.; Bacsa, R. R.; Rousset, A. Specific Surface Area of Carbon Nanotubes and Bundles of Carbon Nanotubes. *Carbon* **2001**, *39*, 507−514.

(5) Schlapbachand, L.; Züttel, A. Hydrogen-Storage Materials for Mobile Applications. *Nature* **2001**, *414*, 353−358.

(6) Huang, X.; Yin, Z.; Wu, S.; Qi, X.; He, Q.; Zhang, Q.; Yan, Q.; Boey, F.; Zhang, H. Graphene-Based Materials: Synthesis, Characterization, Properties, and Applications. *Small* **2001**, *7*, 1876−1902.

(7) Tang, Y.; Yang, D.; Qin, F.; Hu, J.; Wang, C.; Xu, H. Decorating Multi-Walled Carbon Nanotubes with Nickel Nanoparticles for Selective Hydrogenation of Citral. *J. Solid State Chem.* **2009**, *182*, 2279−2284.

(8) Xie, J.; Wang, S.; Aryasomayajula, L.; Varadan, V. K. Platinum Decorated Carbon Nanotube for Highly Sensitive Amperometric Glucose Sensing. *Nanotechnology* **2007**, *18*, 065503−065580.

(9) Girishkumar, G.; Vinodgopal, K.; Kamat, P. V. Carbon Nanostructures in Portable Fuel Cells: Single-Walled Carbon Nanotube Electrodes for Methanol Oxidation and Oxygen Reduction. *J. Phys. Chem. B* **2004**, *108*, 19960−19966.

(10) Karousis, N.; Tsotsou, G. E.; Evangelista, F.; Rudolf, P.; Ragoussis, N.; Tagmatarchis, N. Carbon Nanotubes Decorated with Palladium Nanoparticles: Synthesis, Characterization, and Catalytic Activity. *J. Phys. Chem. C* **2008**, *112*, 13463−13469.

(11) Afanasov, I. M.; Shornikova, O. N.; Avdeev, V. V.; Lebedev, O. I.; Tendeloo, G. V.; Matveev, A. T. Expanded Graphite as a Support for Ni/Carbon Composites. *Carbon* **2009**, *47*, 513−518.

(12) Wang, S. F.; Xie, F.; Hu, R. F. Carbon-Coated Nickel Magnetic Nanoparticles Modified Electrodes as a Sensor for Determination of Acetaminophen. *Sens. Actuators, B* **2007**, *123*, 495−500.

(13) Dao, V. D.; Larina, L. L.; Jung, K. D.; Lee, J. K.; Choi, H. S. Graphene-NiO Nanohybrid Prepared by Dry Plasma Reduction as a Low-Cost Counter Electrode Material for Dye-Sensitized Solar Cells. *Nanoscale* **2014**, *6*, 477−482.

(14) Hsieh, C. T.; Chou, Y. W.; Lin, J. Y. Fabrication and Electrochemical Activity of Ni-Attached Carbon Nanotube Electrodes for Hydrogen Storage in Alkali Electrolyte. *Int. J. Hydrogen Energy* **2007**, *32*, 3457−3464.

(15) Gaboardi, M.; Bliersbach, A.; Bertoni, G.; Aramini, M.; Vlahopoulou, G.; Pontiroli, D.; Mauron, P.; Magnani, G.; Salviati, G.; Züttel, A.; Ricco, M. Decoration of Graphene with Nickel Nanoparticles: Study of the Interaction with Hydrogen. *J. Mater. Chem. A* **2014**, *2*, 1039−1046.

(16) Dong, X.; Li, B.; Wei, A.; Cao, X.; Chan-Park, M. B.; Zhang, H.; Li, L. J.; Huang, W.; Chenb, P. One-Step Growth of Graphene−Carbon Nanotube Hybrid Materials by Chemical Vapor Deposition. *Carbon* **2011**, *49*, 2944−2949.

(17) Kim, Y. S.; Kumar, K.; Fisher, F. T.; Yang, E. H. Out-of-Plane Growth of CNTs on Graphene for Supercapacitor Applications. *Nanotechnology* **2012**, *23*, 015301.

(18) Kumar, K.; Kim, Y. S.; Li, X.; Ding, J.; Fisher, F. T.; Yang, E. H. Chemical Vapor Deposition of Carbon Nanotubes on Monolayer Graphene Substrates: Reduced Etching via Suppressed Catalytic Hydrogenation Using C_2H_2. *Chem. Mater.* **2013**, *25*, 3874−3879.

(19) Kim, U. J.; Lee, I. H.; Bae, J. J.; Lee, S.; Han, G. H.; Chae, S. J.; Günes, F.; Choi, J. H.; Baik, C. W.; Kim, S. I.; Kim, J. M.; Lee, Y. H. Graphene/Carbon Nanotube Hybrid-Based Transparent 2D Optical Array. *Adv. Mater.* **2011**, *23*, 3809−3814.

(20) Mani, V.; Chen, S. M.; Lou, B. S. Three Dimensional Graphene Oxide-Carbon Nanotubes and Graphene-Carbon Nanotubes Hybrids. *Int. J. Electrochem. Sci.* **2013**, *8*, 11641−11660.

(21) Chen, S.; Chen, P.; Wang, Y. Carbon Nanotubes Grown in Situ on Graphene Nanosheets as Superior Anodes for Li-Ion Batteries. *Nanoscale* **2011**, *3*, 4323−4329.

(22) Fengab, J. M.; Dai, Y. J. Water-Assisted Growth of Graphene on Carbon Nanotubes by the Chemical Vapor Deposition Method. *Nanoscale* **2013**, *5*, 4422−4426.

(23) Huang, Y.; Liang, J.; Chen, Y. An Overview of the Applications of Graphene-Based Materials in Supercapacitors. *Small* **2012**, *8*, 1805−1834.

(24) Liu, H.; Cheng, G.; Zheng, R.; Zhao, Y. Controlled Growth of Ni Particles on Carbon Nanotubes for Fabrication of Carbon Nanotubes. *J. Mol. Catal. A: Chem.* **2005**, *225*, 233−237.

(25) Darbari, S.; Abdi, Y.; Mohajerzadeh, S. Branched Carbon Nanotubes to Realize a Novel Capacitive Sensor and Actuator Device. *Sens. Actuators, A* **2011**, *167*, 389−397.

(26) Mohammadi, S.; Kolahdouz, Z.; Mohajerzadeh, S. Hydrogenation-Assisted Unzipping of Carbon Nanotubes to Realize Graphene Nano-Sheets. *J. Mater. Chem. C* **2013**, *1*, 1309−1316.

(27) Mohammadi, S.; Kolahdouz, Z.; Darbari, S.; Mohajerzadeh, S.; Masoumi, N. Graphene Formation by Unzipping Carbon Nanotubes Using a Sequential Plasma Assisted Processing. *Carbon* **2013**, *52*, 451−463.
(28) Dang, S.; Gulseren, O.; Ciraci, S. Electronic Structure of the Contact Between Carbon Nanotube and Metal Electrodes. *Appl. Phys. Lett.* **2003**, *83*, 3180−3182.
(29) Deniau, G.; Azoulay, L.; Jégou, P.; Chevallier, G. L.; Palacin, S. Carbon-to-Metal Bonds: Electrochemical Reduction of 2-Butenenitrile. *Surf. Sci.* **2006**, *600*, 675−684.
(30) Zhou, J. H.; Sui, Z. J.; Zhu, J.; Li, P.; Chen, D.; Dai, Y. C.; Yuan, W. K. Characterization of Surface Oxygen Complexes on Carbon Nanofibers by TPD, XPS, and FT-IR. *Carbon* **2007**, *45*, 785−796.
(31) Ci, L.; Xu, Z.; Wang, L.; Gao, W.; Ding, F.; Kelly, K. F.; Yakobson, B. I.; Ajayan, P. M. Controlled Nanocutting of Graphene. *Nano Res.* **2008**, *1*, 116−122.
(32) Elias, A. L.; Botello-Méndez, A. R.; Meneses-Rodríguez, D.; González, V. J.; Ramírez-Gonzalez, D.; Ci, L.; Muñoz-Sandoval, E.; Ajayan, M. P.; Terrones, H.; Terrones, M. Longitudinal Cutting of Pure and Doped Carbon Nanotubes to Form Graphitic Nanoribbons Using Metal Clusters as Nanoscalpels. *Nano Lett.* **2010**, *10*, 366−372.
(33) Zielinski, M.; Wojcieszak, R.; Monteverdi, S.; Mercy, M.; Bettahar, M. M. Hydrogen Storage in Ni Catalysts Supported on Activated Carbon. *Int. J. Hydrogen Energy* **2007**, *32*, 1024−1032.
(34) Zhong, Z. Y.; Xiong, Z. T.; Sun, L. F.; Luo, J. Z.; Chen, P.; Wu, X.; Lin, J.; Tan, K. L. Nanosized Nickel (or Cobalt)/Graphite Composites for Hydrogen Storage. *J. Phys. Chem. B* **2002**, *106*, 9507−9513.
(35) Kuznetsov, V. L.; Usoltseva, A. N.; Chuvilin, A. L.; Obraztsova, E. d.; Bonard, J. M. Thermodynamic Analysis of Nucleation of Carbon Deposits on Metal Particles and Its Implications for the Growth of Carbon Nanotubes. *Phys. Rev. B* **2001**, *64*, 5401−5408.
(36) Kim, T. Y.; Lee, K. R.; Eun, K. Y.; Oh, K. H. Carbon Nanotube Growth Enhanced by Nitrogen Incorporation. *Chem. Phys. Lett.* **2003**, *372*, 603−607.